Solar Energy Materials and Solar Cells 173 (2017) 33–36

Contents lists available at ScienceDirect

Solar Energy Materials and Solar Cells

journal homepage: www.elsevier.com/locate/solmat

On the equilibrium concentration of boron-oxygen defects in crystalline silicon

D.C. Walter[a,*], R. Falster[b], V.V. Voronkov[b], J. Schmidt[a,c]

[a] Institute for Solar Energy Research Hamelin (ISFH), Am Ohrberg 1, 31860 Emmerthal, Germany
[b] SunEdison Semiconductor, Via Nazionale 59, 39012 Merano, Italy
[c] Department of Solar Energy, Institute of Solid-State Physics, Leibniz Universität Hannover, Appelstr. 2, 30167 Hanover, Germany

ARTICLE INFO

Keywords:
Czochralski silicon
Boron-oxygen defects
Carrier lifetime

ABSTRACT

We determine the equilibrium concentration of the BO defect in boron-doped Czochralski-grown silicon after prolonged (up to 150 h) annealing at relatively low temperatures between 200 and 300 °C. We show that after sample processing, the BO concentration has not necessarily reached the equilibrium state. The actually reached state depends on the detailed temperature profile of the last temperature treatment before the light-induced degradation (LID) is performed. For the investigated Cz-Si materials with base resistivities ranging between 0.5 and 2.5 Ω cm, we observe that an annealing step at 200 °C for 50 h establishes the equilibrium, independent of the base resistivity. Experiments performed at different temperatures reveal that the equilibrium defect concentration decreases with increasing annealing temperature. This observation can be understood, assuming a mobile species which is distributed between at least two different sinks. A possible defect model is discussed.

1. Introduction

In boron-doped and oxygen-rich silicon, the carrier lifetime is limited by a recombination centre which is related to a defect complex containing both of these elements, boron and oxygen [1–3]. This BO-related defect complex reveals its recombination-active properties under illumination at room temperature, leading to a degrading lifetime upon illumination over several hours, if started from a recombination-inactive defect state. This effect is often referred to as light-induced degradation (LID), although the excess electron concentration is actually causing the degradation rather than photons [4]. The recombination-inactive state, corresponding to a high carrier lifetime, can be reached by annealing the samples in darkness, e.g. at 200 °C for 10 min. However, this high lifetime – in the following denoted τ_0 – is not stable upon renewed illumination but degrades again towards the degraded lifetime value τ_d. As it was shown previously, the switching between these two states is completely reversible [2].

Within this paper, we show that the lifetime τ_d and, hence, also the effective defect concentration N_d^*, may change upon annealing the samples at relatively low temperatures between 200 and 300 °C, if the responsible defect complex has not reached an equilibrium. Interestingly, the time span needed to reach this equilibrium, which we determine in this study to be around 50 h, is independent of the doping concentration of the silicon sample for doping concentrations between 5.7×10^{15} cm^{-3} and 3.3×10^{16} cm^{-3}. Additionally, we observe that the equilibrium defect concentration $N_{d,eq}^*$ depends on the annealing temperature applied to reach the equilibrium. We explain the results presented here within the framework of a defect model which consists of a mobile species which is distributed between two different sinks. One of these sinks forms together with the mobile species the BO-related defect complex, while the other sink features no or only minor recombination properties.

2. Experimental details

We use boron-doped Cz-Si wafers with different base resistivities ranging between 0.5 and 2.5 Ω cm. The wafers are cut into samples of either 2.5 × 2.5 cm^2 or 5.0 × 5.0 cm^2 in size. Sample processing includes the removal of the surface damage using an aqueous solution of KOH. After sample cleaning in a standard RCA cleaning sequence, all samples undergo a phosphorus diffusion (847 °C for 51 min), which results in n^+-regions with a sheet resistance of 100 Ω/□ on both wafer surfaces. Subsequently, the phosphosilicate glass (PSG) and the n^+-regions are removed using HF and KOH, respectively. After another RCA cleaning, the surfaces of the samples are passivated by the deposition of 10 nm Al_2O_3 via plasma-assisted atomic layer deposition. Finally, the samples are annealed at 425 °C for 15 min in ambient environment to activate the Al_2O_3 surface passivation [5].

* Corresponding author.
E-mail address: d.walter@isfh.de (D.C. Walter).

http://dx.doi.org/10.1016/j.solmat.2017.06.036
Received 31 March 2017; Received in revised form 16 June 2017; Accepted 19 June 2017
Available online 03 July 2017

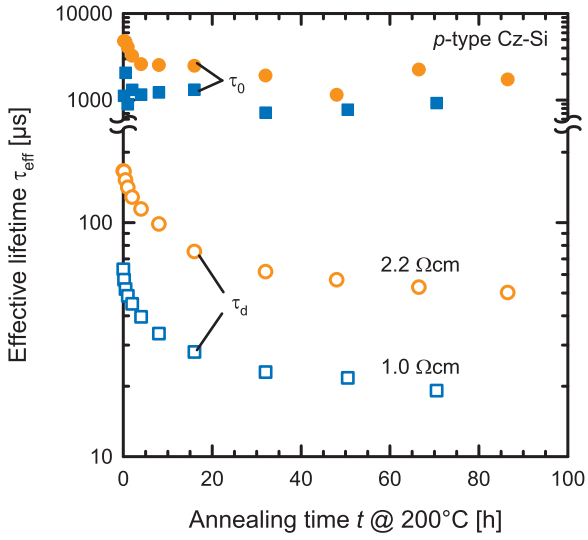

Fig. 1. Measured effective lifetimes τ_{eff} of two samples with a resistivity of 2.2 Ω cm (orange circles) and 1.0 Ω cm (blue squares) plotted versus the annealing time t at 200 °C. The lifetimes after annealing in darkness τ_0 (full symbols) and after complete LID τ_d (open symbols) are shown. Over the course of 80 h annealing τ_d shows an exponential degradation. (For interpretation of the references to color in this figure legend, the reader is referred to the web version of this article.)

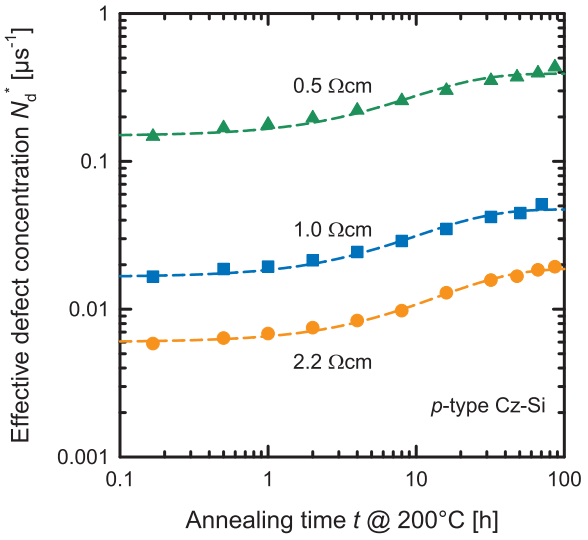

Fig. 2. Effective defect concentration N_d^* of three lifetime samples with different base resistivities (triangles: 0.5 Ω cm, squares 1.0 Ω cm and circles: 2.2 Ω cm) plotted versus the annealing time t at 200 °C. Please note, the values of the 0.5 Ω cm sample are extracted at $\Delta n = 0.5\times10^{14}$ cm^{-3} otherwise an injection level of $\Delta n/p_0 = 0.1$ is chosen. The dashed lines are mono-exponential fits of the data points.

Lifetime measurements are performed using the lifetime tester WCT-120 from Sinton Instruments. If not stated otherwise, all lifetimes in the following are extracted at $\Delta n = 0.1\times p_0$, with the excess carrier density Δn and the hole concentration in darkness p_0.

3. Results and discussion

3.1. Adjusting the equilibrium

In Fig. 1, the change of the lifetimes τ_0 and τ_d upon annealing at 200 °C is shown for two different samples with 1.0 and 2.2 Ω cm base resistivity. After each annealing step, the lifetime τ_0 is measured. Afterwards, the lifetime samples are illuminated at 40 °C for 20 h, using a halogen lamp with an illumination intensity of $P_{ill} = 10$ mW/cm^2, to reach the fully degraded state. Then, the lifetime τ_d is measured. As can be seen from Fig. 1, the lifetime after annealing remains almost stable on a very high level, higher than 700 µs for the 1.0 Ω cm material and higher than 1.9 ms for the 2.2 Ω cm. Hence, we conclude that the surface passivation quality remains on a high and stable level during the course of the experiment. This interpretation is further supported by float-zone (FZ-Si) wafers processed in parallel. On the 1.3 Ω cm FZ-Si wafers we measure a slight degradation from 2.6 to 1.6 ms over the course of 80 h annealing at 200 °C. The lifetime after complete LID, τ_d, however, shows an exponential decay until a saturation value $\tau_{d.eq}$ is reached.

From the measured lifetimes τ_d and τ_0 we calculate the effective defect concentration using the equation $N_d^* = \tau_d^{-1} - \tau_0^{-1}$. Fig. 2 shows the evolution of the effective defect concentration upon annealing at 200 °C. For all examined materials, we observe an exponential increase of the defect concentration until a saturation value $N_{d.eq}^*$ is reached. The dashed lines in Fig. 2 are mono-exponential fits of the form $N_d^* = y_0 + a\times(1-\exp(-\gamma \times t))$, with γ being the equilibration rate constant. We find a rate constant of $\gamma(200°C) = (0.06 \pm 0.01)\,h^{-1}$ independent of the base doping concentration.

On another set of lifetime samples, we examine the defect concentration on an even longer time scale by annealing the samples subsequently three times for 50 h at 200 °C and determine N_d^* after 50 h, 100 h and 150 h. Fig. 3 shows N_d^* plotted versus the annealing time at 200 °C for three different samples with base resistivities ranging between 0.5 and 2.5 Ω cm. In-between the lifetime measurements of τ_0 and τ_d after each annealing step, the samples are illuminated at room temperature longer than 100 h using a halogen lamp with an illumination intensity of $P_{ill} = 10$ mW/cm^2. For annealing times longer than 50 h no change of N_d^* can be observed for these samples. This suggests that the equilibrium state – characterized by the equilibrium defect concentration $N_{d.eq}^*$ – is reached within 50 h of annealing time for all samples, independent of the base resistivity.

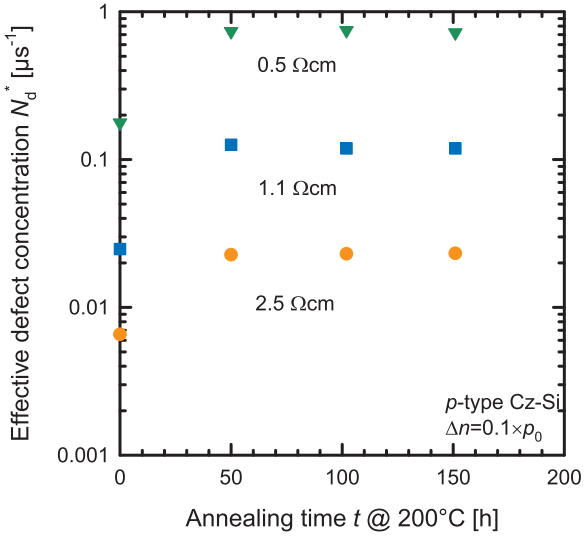

Fig. 3. Effective defect concentration N_d^* plotted versus annealing time t at 200 °C in darkness for three different samples with different base resistivities. The equilibration process proceeds within the first 50 h of annealing. Longer annealing has no further effect on N_d^*, hence the equilibrium defect concentration $N_{d.eq}^*$ is reached after 50 h of annealing.

3.2. Temperature-dependent defect equilibrium

In addition, we examine the temperature dependence of the equilibrium defect concentration $N_{d.eq}^*$ by annealing the same samples in darkness for 50 h at different temperatures in the following sequence: 240 °C, 220 °C, 200 °C and 300 °C. At the end of this sequence, we add additionally a short annealing step at 425 °C for 15 min. We added this short annealing step to compare the defect concentration measured

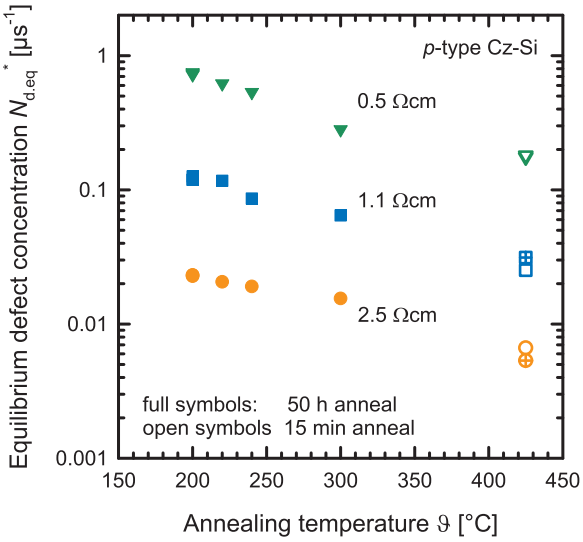

Fig. 4. Equilibrium defect concentration $N_{d,eq}^*$ versus annealing temperature ϑ. $N_{d,eq}^*$ decreases with increasing temperature. Full symbols correspond to $N_{d,eq}^*$ after annealing at the respective temperature for 50 h, open symbols correspond to the defect concentration after annealing for 15 min at 425 °C before and after the annealing sequence. Crossed symbols mark the last measurement in the sequence.

before and after the complete annealing sequence with an identical temperature treatment right before the measurement.

In Fig. 4, the equilibrium defect concentrations $N_{d,eq}^*$ (full symbols) are plotted versus the annealing temperature. The open symbols correspond to N_d^* after annealing for 15 min at 425 °C before and after the annealing sequence. For all examined materials $N_{d,eq}^*$ decreases following an Arrhenius law with increasing temperature.

In the context of the well-known lifetime parameterization due to the formation of BO-related defects by Bothe et al. [6], the decreasing lifetime after illumination as shown in Fig. 1 can be interpreted as a decreasing enhancement factor, which was introduced to describe the lifetime limit after an additional high-temperature treatment (e.g. a phosphorus diffusion step). Therefore, care has to be taken when determining the fundamental lifetime limit based on Bothe's parameterization, as the enhancement factor depends on the actual sample process and can therefore deviate for the same material when different processes are applied.

3.3. Defect model describing the defect equilibrium

The temperature dependence of the equilibrium defect concentration can be understood if a BO latent defect (which reconstructs into a recombination-active configuration in the presence of excess electrons, thus, leading to the lifetime degradation) is composed of a BO immobile core (BO_{core}) and a mobile species X [7]. The X species could be an interstitial boron atom B_i, while the core could be a BO complex of a substitutional boron atom and an interstitial oxygen atom. More generally, X may be an interstitial impurity; in that case the core would be a B_sO_2 defect, to account for the established proportionality of the defect concentration to the substitutional boron concentration [B_s] and the squared interstitial oxygen concentration $[O_i]^2$ [8]. As the absolute concentration of the BO-related defects is not known, also metal impurities (like for instance Ni_i or Cu_i) maybe reasonable candidates for X, even if their concentration is below the detection limit of trace analysis. The X species are present mostly in a form of nano-precipitates (NPs) [7]. The free X species (of a concentration C) and those trapped by BO_{core} defects (of a concentration C^*) are assumed to co-exist in equilibrium, according to the mass-action law for a standard reaction $X + BO_{core} \rightarrow XBO_{core}$:

$$C(N - C^*)/C^* = K, \tag{1}$$

where N is the total concentration of the core defects and $(N - C^*)$ is the concentration of those non-occupied by species X; K is the equilibrium reaction constant.

Within this model, a prolonged dark anneal leads to equilibration between X species with the NPs – a process in which C finally approaches the solubility value C_e – that corresponds to the equilibrium between dissolved free X species and the NPs. The solubility C_e is an Arrhenius-type function of T:

$$C_e = A \times \exp(-E_s/k_B T) \ . \tag{2}$$

This expression is directly applicable for a neutral X species (like Ni_i). For a single-positive X defect (like B_i or Cu_i), the solubility is proportional to the hole concentration p (which is close to the boron concentration in our samples). As C approaches the solubility, the final concentration C^* of the XBO_{core} latent defects, which is directly proportional to the effective equilibrium defect concentration $N_{d,eq}^*$, reaches according to Eq. (1) the equilibrium value:

$$C_e^* = C_e N/(C_e + K) \ . \tag{3}$$

This is a temperature-dependent quantity provided that $C_e \ll K$. This inequality means that the occupancy of traps (BO_{core} defects) by the X-species is low, most of BO defects are not occupied, and $C^* \ll N$ by Eqs. (1) and (3). With this assumption, the concentration C^* of trapped species (of the latent XBO_{core} centres, converted into SRC by illumination) is proportional to C. In that case, C_e^* is proportional to the concentration N of the core BO defects (independent of T) and to a temperature-dependent ratio C_e/K. The equilibrium constant K is an Arrhenius-type quantity proportional to $\exp(-E_b/k_B T)$ (where E_b is the binding energy between X and BO_{core}). Accordingly, from Eq. (3) the temperature dependence of C_e^* can be derived:

$$C_e^* \propto N \times (C_e/K), \tag{4}$$

with $(C_e/K) \propto \exp(-E_s / k_B T) / \exp(-E_b / k_B T) = \exp(-\Delta E / k_B T)$. In effect, C_e^* is an Arrhenius-type function of T with the activation energy $\Delta E = E_s - E_b$.

Fig. 5 shows an Arrhenius-like plot where $N_{d,eq}^*$ is plotted versus the inverse temperature $1/T$. The coloured dashed lines are fits of the defect concentrations using Eq. (4), agreeing very well with the prediction. From these fits $\Delta E = (-0.16 \pm 0.03)$ eV is obtained. The fact that ΔE is negative implies that the binding energy E_b of species X to BO_{core} is larger than the dissolution energy E_s of species X from the nano-precipitates by about 0.16 eV. Interestingly, the defect concentration extracted after annealing at 425 °C agrees well with the Arrhenius fit. This suggests that an annealing at 425 °C for 15 min is sufficient to establish the equilibrium. Please note, however, that annealing at 425 °C for a shorter time span or at a lower temperature for 15 min would not have established the corresponding temperature-dependent defect equilibrium.

According to this model, the equilibrated defect concentration C_e^* is proportional to $C_e \times N$ – and thus proportional to the boron concentration N_B, if the X species is neutral, or to $p \times N_B$, if the species is positively charged. From Fig. 5 it can be extracted that the equilibrium defect concentration $N_{d,eq}^*$ and, hence, C_e^* increases upon increasing N_B (decreasing resistivity) but super-linearly, which maybe – within this model – a hint towards a positively charged species X like B_i^+ or Cu_i^+. Further experiments are necessary to clarify this point.

The initial defect concentration $C^*(0)$, being directly proportional to the effective defect concentration N_d^* prior to the equilibration process, depends on the thermal history. According to the defect model described above, the relaxation from $C^*(0)$ to the final equilibrium value C_e^* proceeds by the kinetic equation [9]

$$dC_{tot}/dt = -4\pi R_{np} N_{np} D_X (C - C_e) \ , \tag{5}$$

where C_{tot} is the total concentration of X species – free and trapped by all existing trapping defects (including the BO_{core} defects), R_{np} and N_{np} is the radius and density of NPs, and D_x is the diffusivity of species X.

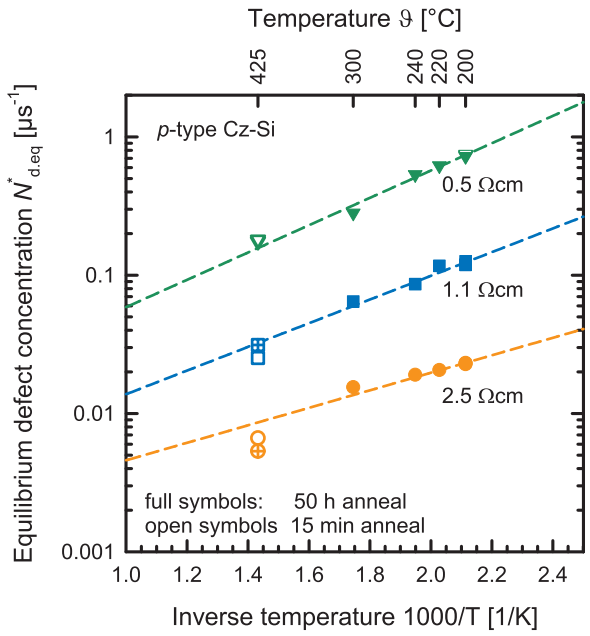

Fig. 5. Equilibrium defect concentration $N^*_{d,eq}$ versus inverse annealing temperature $1/T$. Full symbols correspond to $N^*_{d,eq}$ after annealing at the respective temperature for 50 h, open symbols correspond to the defect concentration after annealing for 15 min at 425 °C before and after the annealing sequence. Crossed symbols mark the last measurement in the sequence. The coloured dashed lines are fits of Eq. (3) to the data, which results in $\Delta E = (-0.16 \pm 0.03)$ eV. (For interpretation of the references to color in this figure legend, the reader is referred to the web version of this article.)

Using again the inequality $C_e \ll K$, this kinetic equation is linear, in accordance with the experimentally observed single-exponential relaxation presented in Fig. 2. Otherwise, the $C^*(t)$ dependence would be complicated (non-linear). Additionally, if the BO_{core} were the major traps for X, then C_{tot} would be equal to $C + C^*$ − approximately to $C^* = C\,N\,/K$. Then, the rate constant would be inversely proportional to the concentration of BO_{core}, N, and, hence, to the boron concentration N_B. As it is shown in Fig. 2 and Fig. 3, this is clearly not the case – by our results the rate constant is independent on N_B. It can be thus concluded that, in our model proposed above, the major trap for X would not be BO_{core} but some other defect not involving boron. A possible candidate for this major trap would for example be oxygen. In other words, the X species would be represented mostly by the non-recombination active XO rather than by the recombination-active XBO_{core}. The rate constant is then expected to be inversely proportional to the oxygen concentration $[O_i]$, which needs to be tested in future experiments using lifetime samples with strongly varying oxygen concentrations.

3.4. Context to previous BO defect models

In the model of Ref. [10], the presumed dependence of the saturated SRC concentration on the hole concentration p – rather than on the boron concentration N_B in compensated samples – was explained assuming that the latent defect (future SRC) involves a mobile component – a positively charged interstitial boron B_i. These species are mostly precipitated at an earlier stage of sample cooling, forming nano-precipitates (NPs). Then, the NPs supply B_i up to the solubility proportional to the hole concentration p, and these dissolved B_i are attached to some core defects, assumed at that time to be oxygen dimers. Later it was realized [7] that the core may be more complicated, like BO – a complex of a substitutional boron atom and an oxygen atom – and that the mobile species of the defect might not necessarily be B_i but any positively charged impurity like e.g. Cu supplied from copper NPs up to the solubility proportional to p. In a more recent publication [11] the correlation of SRC with p was questioned in favor of a simple correlation to the boron concentration N_B. In that case, a very simple composition of SRC, just BO_2, was regarded more likely.

The data of the present paper – showing a pronounced change in the SRC concentration upon annealing at low temperatures, around 200 °C – are forcing us to return to the concept of the SRC recombination centre involving a mobile component X attached to a core boron-oxygen defect BO_{core} (which may be BO, or BO_2, or boron-free O_2). This X-species may be either B_i or any fast-diffusing interstitial impurity like positive Cu or neutral Ni. In other words, the chemical composition of the latent defects, future SRC, is XBO_{core}. A change in the SRC concentration induced by a low-temperature annealing can be then explained in a straightforward way, as an exchange of X-species between the BO_{core} defects and the NPs (which are the source/sink of X-species).

4. Summary

Within this paper, we have shown that the boron-oxygen-related defect concentration has not necessarily reached an equilibrium after sample processing. However, an equilibrium can be established if the samples are annealed in darkness. We have observed that 200 °C at 50 h of annealing in darkness is sufficient to establish the equilibrium, independent of the specific resistivity of the samples under investigation between 0.5 and 2.5 Ω cm. In addition, we have shown that this equilibrium is temperature-dependent: higher annealing temperatures lead to lower equilibrium defect concentrations. The temperature dependence of the equilibrium defect concentration can be understood within a defect model which consists of a mobile species, which is distributed between at least two sinks. One of these sinks forms together with the mobile species the recombination-active defect centre, while the other sink features no or only minor recombination properties.

Acknowledgements

This work was funded by the German State of Lower Saxony, SunEdison Semiconductor and the German Federal Ministry of Economics and Energy (BMWi) within the research project “SolarLIFE” (contract no. 0325763C). The content is the responsibility of the authors.

References

[1] H. Fischer, W. Pschunder, Investigation of photon and thermal induced changes in silicon solar cells, in: Proceedings of the 10th IEEE PVSC, Palo Alto, CA (IEEE, New York, 1973), 1974, 404.
[2] J. Schmidt, A.G. Aberle, R. Hezel, Investigation of carrier lifetime instabilities in Cz-grown silicon, Proceedings of the 26th IEEE PVSC, Anaheim, CA, (IEEE, New York, 1997), 1997, 13.
[3] S.W. Glunz, S. Rein, W. Warta, J. Knobloch, W. Wettling, On the degradation of Cz-Silicon solar cells, in: Proceedings of the 2nd WC-PVSEC, Vienna, Austria, (WIP, Munich, 1998), 1998, 1343.
[4] J. Knobloch, S.W. Glunz, D. Biro, W. Warta, E. Schaffer, W. Wettling, Solar cells with efficiencies above 21% processed from Czochralski grown silicon, in: Proceedings of the 25th IEEE PVSC, Washington DC, (IEEE, New York, 1997), 1996, 405–408.
[5] F. Werner, B. Veith, V. Tiba, P. Poodt, F. Roozeboom, R. Brendel, J. Schmidt, Very low surface recombination velocities on p- and n-type c-Si by ultrafast spatial atomic layer deposition of aluminum oxide, Appl. Phys. Lett. 97 (2010) 162103.
[6] K. Bothe, R. Sinton, J. Schmidt, Fundamental boron-oxygen-related carrier lifetime limit in mono- and multicrystalline silicon, Prog. Photo.: Res. Appl. 13 (2005) 287–296.
[7] V.V. Voronkov, R. Falster, Light-induced boron-oxygen recombination centres in Silicon: understanding their formation and elimination, Solid State Phenom. (SSP) 205–206 (2013) 3–14.
[8] J. Schmidt, K. Bothe, Structure and transformation of the metastable boron- and oxygen-related defect center in crystalline silicon, Phys. Rev. B 69 (2004) 24107.
[9] V.V. Voronkov, R. Falster, B. Lim, J. Schmidt, Permanent recovery of electron lifetime in pre-annealed silicon samples: a model based on Ostwald ripening, J. Appl. Phys. 112 (2012) 113717.
[10] V.V. Voronkov, R. Falster, K. Bothe, B. Lim, J. Schmidt, Lifetime-degrading boron-oxygen centres in p-type and n-type compensated silicon, J. Appl. Phys. 110 (2011).
[11] V.V. Voronkov, R. Falster, Permanent deactivation of boron–oxygen recombination centres in silicon, Phys. Status Solidi (b) 253 (2016) 1721–1728.